water

MDPI

Article

Hydraulic and Technological Investigations of a Phenomenon Responsible for Increase of Major Head Losses in Exploited Cast-Iron Water Supply Pipes

Piotr Wichowski [1,*], Marek Kalenik [1], Agnieszka Lal [2], Dariusz Morawski [1] and Marek Chalecki [3]

[1] Institute of Environmental Engineering, Warsaw University of Life Sciences—SGGW, Nowoursynowska 159, 02-776 Warsaw, Poland; marek_kalenik@sggw.edu.pl (M.K.); dariusz_morawski@sggw.edu.pl (D.M.)
[2] Faculty of Civil Engineering and Architecture, Lublin University of Technology, Nadbystrzycka 40, 20-618 Lublin, Poland; a.lal@pollub.pl
[3] Institute of Civil Engineering, Warsaw University of Life Sciences—SGGW, Nowoursynowska 159, 02-776 Warsaw, Poland; marek_chalecki@sggw.edu.pl
* Correspondence: piotr_wichowski@sggw.edu.pl; Tel.: +48-22-5935154

Abstract: The paper presents results of investigations of influence of major head losses on exploitation properties of water supply pipes after 30-year exploitation. The tested materials were cast-iron pipes with the internal diameter of 150 mm. A flowability drop coefficient η_t with average value of 0.45 was determined. Using the measured values of pressure difference Δp determined the absolute roughness of internal walls of the pipes after 30-year exploitation, which was referred to the new pipelines. The absolute roughness for the exploited pipes was equal to k = 27.6 mm, whereas for the new ones it was significantly lower and equal to k = 0.9 mm. Additionally, an analysis of the chemical and mineral composition of sediments gathered in the investigated pipelines was also performed. The top layer of the sediments was dominated by the compounds of a character of the iron hydroxide: goethite (α-FeOOH) and lepidocrocite (γ-FeOOH), whereas the internal layer was supplemented by the gypsum and sulfur, which was proven by the investigations performed with the use of scanning electron microscope (SEM). The sediment gathered within the pipes is the main reason of ca. 30-fold increase of the absolute roughness, which resulted in the flowability drop of the exploited water supply pipes.

Keywords: water supply network pipes; cast-iron pipes; major head losses; corrosion; absolute roughness; relative roughness; XRD; SEM

Citation: Wichowski, P.; Kalenik, M.; Lal, A.; Morawski, D.; Chalecki, M. Hydraulic and Technological Investigations of a Phenomenon Responsible for Increase of Major Head Losses in Exploited Cast-Iron Water Supply Pipes. *Water* **2021**, *13*, 1604. https://doi.org/10.3390/w13111604

Academic Editor: Pedro L. Iglesias Rey

Received: 30 April 2021
Accepted: 3 June 2021
Published: 6 June 2021

1. Introduction

The basic task of a water supply network is to deliver water in an appropriate quantity and at the appropriate pressure to all connected users [1]. The water supply network should ensure high-quality water to all categories of consumers [2–5] at low costs of construction and exploitation of the network. Especially in water supply networks made of steel and cast-iron pipes, hydraulic flow conditions can deteriorate during long-lasting exploitation. This phenomenon is caused by an incrustation of pipe walls by sediments precipitating from water or being a product of pipe corrosion [6,7], sometimes being so-called hydrobiological accretion [8–11]. It leads to a recurring pollution of the treated water in the water supply system [12,13] as well as reduction and deformation of the cross-section area of the pipelines. Along with the exploitation time of a cast-iron pipeline, the absolute roughness k of its internal wall increases [14–17].

Corrosion, especially that of cast-iron pipes, has been emphasized as the most frequent exploitation problem in water supply networks [18,19]. Data gathered by the United States Environmental Protection Agency [20] estimate the total length of pipelines in USA as over 2,000,000 miles. According to investigations by the American Water Works Association [21,22], 22.5% of these pipes are directly concerned by the corrosion, including

cast iron without lining (14.4%), spheroidal cast iron without lining (4.3%) and steel (3.8%). An additional 34.1% of pipes can be indirectly concerned by the deterioration of state of their lining: cement-lined spheroidal iron cast (19.7%) and cement-lined iron cast (14.4%). Similar proportions are expected in other countries, which emphasizes a potential influence of this problem for operators of potable water distribution systems worldwide [23].

From a hydraulic aspect, one can observe high-pressure line slopes and problems in ensuring appropriate pressure at hydraulic connections to the network users. High-pressure line slopes affect energy consumption and exploitation costs of the water distribution systems.

A hydraulic efficiency of a pipeline being exploited for t years can be determined with three methods: using a major head loss coefficient λ_t, hydraulic resistivity C_t or specific flowability M_t [24,25]. Values of λ_t can be calculated from the classical Colebrook-White formula [26] or its numerous modifications [27–30]. Resistivity increase or flowability decrease in a pipeline being exploited for t years are characterized by the resistivity rise coefficient δ_t (1) or flowability drop coefficient η_t (2).

$$\delta_t = \frac{C_t}{C_o} = \frac{\lambda_t}{\lambda_o}\left(\frac{d_o}{d_t}\right)^5 \quad (1)$$

$$\eta_t = \frac{M_t}{M_o} = \frac{1}{\sqrt{\frac{\lambda_o}{\lambda_t}\left(\frac{d_t}{d_o}\right)^5}} \quad (2)$$

where:

δ_t—resistivity rise coefficient of a pipeline after t years of exploitation;
η_t—flowability (efficiency) drop coefficient of a pipeline after t years of exploitation;
C_o, C_t—resistivity of a new pipeline and a pipeline after t years of exploitation, s^2/m^6;
M_o, M_t—flowability of a new pipeline and a pipeline after t years of exploitation, s^2/m^6;
λ_o, λ_t—friction loss coefficient of a new pipeline and a pipeline after t years of exploitation;
d_o, d_t—internal diameter of a new pipeline and equivalent diameter of a pipeline after t years of exploitation.

In the accessible technical literature, there are few new publications concerning issues of experimental determination of hydraulic losses during flow of Newtonian liquids [31–34]. Currently, the researchers deal first of all with mathematical modeling of flow structures in various Newtonian or non-Newtonian liquids using the CFD software (Computational Fluid Dynamics) [35–39].

The problem of deterioration of hydraulic flow conditions, i.e., increase of hydraulic losses, sediment accumulation and corrosion development in water supply network pipelines, has been an object of numerous research studies. The process of pipe ageing can be described by reduction of the pipe diameter or increase of the pipe roughness. Some researchers took only the influence of exploitation time into account [40,41], while others additionally considered pipe diameters [42,43] or water quality [23,44]. There is a real need for more exact measurements in operational and/or laboratory conditions in aim to define realistic age-affected changes of the roughness and diameter of the pipes so that the results of these measurements can be used for modeling water supply systems using old pipelines [17]. The accessible literature contains formulas for calculation of pipe roughness after t years of exploitation [15,45,46], whereas Kandlikar et al. provided a simplified formula for calculation of an equivalent diameter after t years of exploitation [47]. In the publications, there is no information concerning structure and chemical composition of the gathered sediments. Knowledge about their chemical composition and structure is important from the point of view of a choice of appropriate chemical reagents which would allow solving the sediments and renovation of the pipelines with reduced flowability.

The objective of the paper is the analysis of the experimental investigations on the influence of 30-year exploitation of cast-iron pipes on the roughness increase, flowability decrease and chemical composition of the gathered sediments.

2. Materials and Methods

The investigations were performed for cast-iron pipes which had worked in a water supply network, exploited for 30 years. Note that 2 m long sections of pipeline were used for the investigations. With the aim of comparing results of investigations, measurements were performed for a new pipe and three pipes after 30-year exploitation (Figure 1).

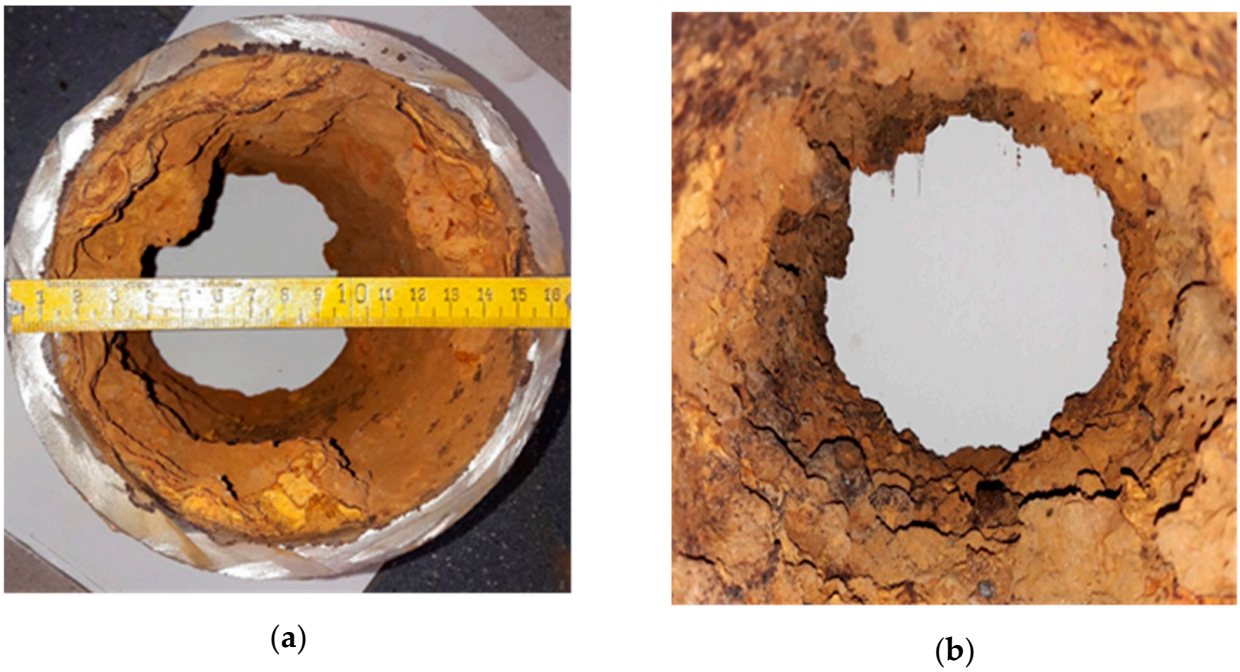

(**a**) (**b**)

Figure 1. Cast-iron pipe after 30 years of exploitation: (**a**) Pipe cross section; (**b**) Sediments accumulated during the pipe exploitation.

The investigations were performed on a test rig presented in Figure 2. The pump (2) leads water through the pipeline (2), to the cast-iron pipe section (8) being investigated and then, through the draining pipe (17) to the sewerage outlet. The flow rate measurements were performed with use of the PROMAG 53 electromagnetic water flow meter (3), the hydraulic losses were measured with use of the DELTABAR S pressure difference meter (12), the temperature—with the TMR31 thermometer (6). Due to sensitivity of the devices and fast variability of readings resulting from flow pulsation, the readings were registered with a time step 1 s with use of the Endress+Hauser's RSG40 data logger (16). Changes in the flow rate were measured with use of the needle valve (4). The investigated pipe sections (8) were butt-joined by the metal repairing bands (7) with an internal sealing rubber surface. The internal diameter of the investigated pipe sections was equal to 150 mm, whereas that of the water supplying and draining pipe—50 mm. Before the measuring section, a diffuser was used, after it—a confusor. The impulse hoses and borings were made at distances $L_1 = 5D$ after the diffuser as well as $L_2 = 3D$ before the confusor. It is concordant to the assembly directives of Endress + Hauser, related to the DELTABAR S pressure difference meter, where the manufacturer submits the requirements of the standard DIN 19210 [48]. In analogical way, the condition of rectilinearity of the pipe section before and after the PROMAG 53 flow meter was fulfilled.

The investigations were performed in 4 rounds, i.e., a zero round for the new pipe as well as three rounds for the pipes being exploited. The measurements were repeated three times for each pipe. The flow rates were assumed within the range 5–40 $m^3\ h^{-1}$ with step 5 $m^3\ h^{-1}$.

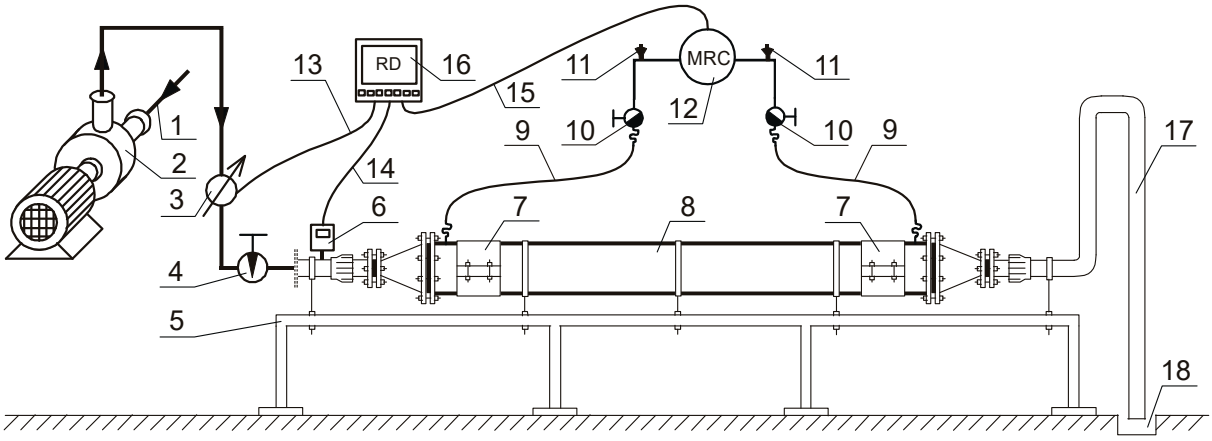

Figure 2. Scheme of a test rig for investigations of major head losses in pipes: 1—water supplying pipe; 2—pump; 3—electromagnetic water flow meter; 4—needle valve controlling water flow rate; 5—frame carrying pipes; 6—thermometer; 7—clamping sleeves; 8—cast-iron pipe; 9—impulse hoses; 10—cut-off ball valves; 11—breathers; 12—piezoelectric pressure difference meter; 13, 14, 15—control cable; 16—data logger; 17—draining pipe; 18—outlet to sewerage.

The standard method of calculation of pressure difference between a water flow through a circular cross section pressure pipeline consists in application of the Darcy–Weisbach formula [5]:

$$\Delta p = \left(\Sigma\xi + \frac{\lambda l}{d}\right)\frac{8Q^2\rho}{\pi^2 d^4} \quad (3)$$

where:

Δp—pressure difference in the investigated pipeline section, Pa;
$\Sigma\xi$—sum of the local hydraulic loss coefficients;
λ—major head loss coefficient;
l—pipeline length, m;
d—pipeline diameter, m;
Q—flow rate, m^3/s;
ρ—water density, kg/m^3.

During a water flow through a rectilinear pipeline section ($\Sigma\zeta = 0$), the major head loss coefficient λ is calculated from the Colebrook–White formula:

$$\frac{1}{\sqrt{\lambda}} = -2log\left(\frac{2.51}{Re\sqrt{\lambda}} + \frac{\varepsilon}{3.71}\right) \quad (4)$$

where:

Re—Reynolds number;
ε—relative roughness.

A relative roughness ε is described by a formula:

$$\varepsilon = \frac{k}{d} \quad (5)$$

where:

k—absolute roughness of an internal wall of the pipeline, [m].

whereas the Reynolds number can be calculated as:

$$Re = \frac{4Q}{\pi d\nu} \quad (6)$$

where:

υ—kinematic viscosity coefficient, m^2/s.

The absolute roughness describes a character of unevenness of the internal surface of a pipe and it is assumed according manufacturer data or according to measurements. It is difficult to determine it in pipelines during a normal exploitation because it usually changes due to progressing corrosion processes. Therefore, using Nikuradze's investigations, these values are assumed for individual, predicted cases; their values are given in the standard [49].

The pressure difference Δp, the flow rate Q and the temperature of flowing water were measured and registered automatically. The major head loss coefficient λ has been calculated according to Form, (3) which was transformed with respect to the parameter λ:

$$\lambda = \frac{\Delta P \pi^2 d^5}{8Q^2 \rho l} \tag{7}$$

Using Formulas (4–6), it has been derived a formula (8) allowing calculation of the absolute roughness k of the investigated pipes:

$$k = 3.71\left(10^{-\frac{1}{2\sqrt{\lambda}}} - \frac{2.51}{Re\sqrt{\lambda}}\right)d \tag{8}$$

Knowing the roughness of the tested pipes and using a formula proposed by Kandlikar et al. [47] the equivalent diameter of a pipeline after t years of exploitation was determined:

$$d_t = d_o - 2k \tag{9}$$

In an aim to identify the character of the process of accumulation of sediments at the internal surfaces of pipes, surface roughness, structure and chemical composition of the sediments gathered in the pipes were also investigated. The 3D investigations of the surface roughness were performed with the use of the Hirox KH-8700 digital microscope (Hirox, Tokyo, Japan).

The chemical composition of the investigated sediments was determined by the energy dispersive X-ray fluorescence method with use of the Panalytical's Epsilon 3 spectrometer (Panalytical, Malvern, United Kingdom)). The tests were carried out in the measurement range for the elements Na ÷ Am on the apparatus equipped with the Rh X-ray tube (9 W, 50 kV, 1 mA), 4096-channel spectrum analyzer, 6 measuring filters (Cu-500, Cu-300, Ti, Al-50, Al-200, Ag) as well as the high-resolution solid-state SDD detector (50 µm thick beryllium window), cooled with a Peltier's cell.

The mineral composition of the sediment was determined with use of the X-ray phase analysis (XRD). Measurements were done with the use of the powder diffraction by means of the Panalytical X'pertPRO MPD X-ray diffractometer with the PW 3020 goniometer (Panalytical, Malvern, UK). As an X-ray radiation source, the copper tube was used (CuKα radiation, α = 1.54178 Å). The diffraction data handling was performed with help of the X'Pert Highscore software. The identification of mineral phases was based on the PDF-2 Release 2010 database, formalized by JCPDS-ICDD.

The morphology of main components of the sediments was determined with the use of the scanning electron microscope (SEM) Quanta 250 FEG from the FEI company (Hillsboro, OR, USA). Additionally, the chemical composition in the microrange of the investigated sediments was determined with use of the energy dispersive X-ray spectroscopy attachment EDS from the EDAX company. The samples were dusted by graphite.

The pipes under investigation had been applied for the transport of underground water taken from quaternary formations with use of bored wells from the depth of 28 m. The physical and chemical characteristic of the water transported by the investigated cast-iron pipes is presented in Table 1.

Table 1. Physical and chemical characteristic of the water transported by the investigated cast-iron.

Determination	Unit	Parameter
Temperature	°C	12.6
Reaction	pH	7.23
Conductivity	$\mu S \cdot cm^{-1}$	666
Color	mg $Pt \cdot dm^{-3}$	3
Turbidity	NTU	0.5
Nitrates	mg $NO_3^- \cdot dm^{-3}$	1.82
Chlorides	mg $Cl^- \cdot dm^{-3}$	70.12
Sulphates	mg $SO_4^{2-} \cdot dm^{-3}$	169.86
Ammonium ion	mg $NH_4+ \cdot dm^{-3}$	0.04
General acidity	mval$\cdot dm^{-3}$	0.54
General basicity	mval$\cdot dm^{-3}$	4.48
General basicity	mg $CaCO_3 \cdot dm^{-3}$	224.2
Alkaline basicity	mval$\cdot dm^{-3}$	0.00
General hardness	mval$\cdot dm^{-3}$	7.81
General hardness	mg $CaCO_3 \cdot dm^{-3}$	390.85
Carbonate hardness	mg $CaCO_3 \cdot dm^{-3}$	224.46
Non-carbonate hardness	mg $CaCO_3 \cdot dm^{-3}$	166.65
Calcium hardness	mval$\cdot dm^{-3}$	6.34
Magnesium hardness	mval$\cdot dm^{-3}$	1.45
Calcium	mg $Ca^{2+} \cdot dm^{-3}$	126.98
Magnesium	mg $Mg^{2+} \cdot dm^{-3}$	17.61
Manganese	mg $Mn^{2+} \cdot dm^{-3}$	0.01
Iron	mg $Fe \cdot dm^{-3}$	0.03
Free CO_2	mg $CO_2 \cdot dm^{-3}$	27.60
Aggressive CO_2	mg $CO_2 \cdot dm^{-3}$	2.86
Dissolved oxygen	mg $O_2 \cdot dm^{-3}$	2.89
COD—$KMnO_4$	mg $O_2 \cdot dm^{-3}$	1.25
Dry residue	mg$\cdot dm^{-3}$	605.43
Residue after roasting	mg$\cdot dm^{-3}$	365.30

A number of methods exist for determination of aggressive and corrosive features of water [50–53]. In aim to determine the corrosive features of water flowing in the investigated pipes, the Langelier Saturation Index (LSI) and the Ryznar Stability Index (RSI) [54–57] were calculated.

3. Results

Figure 3 presents average values of the measured major head losses for the new pipe and the pipe after 30-year exploitation as well as the calculated theoretical pressure losses with the assumption that the maximum values of the absolute roughness coefficient of the pipeline internal wall is equal to k = 1 mm for the new pipe and k = 4 mm for the pipe with significant sediments (according to Table 2 [49]).

The pressure difference values Δp, measured for the new pipes, are very close to the theoretical (calculated) values for the assumed absolute roughness of the internal wall of the pipeline k = 1 mm and they are equal to 98% of the theoretical value on average. The sediments covering the pipe internal wall deteriorate hydraulic flow conditions of the water as well as significantly increase real values of the pressure difference Δp, and it is a correct trend, concordant with the literature data [17,58]. For the analyzed range of water volume flow rate Q, the measured real values of the pressure difference Δp for the pipes after 30-year exploitation are five times higher on average (502%) than the measured real values of the pressure difference Δp for the new pipe. For the pipes after 30-year exploitation, the measured real values of the pressure difference Δp are over threefold higher on average (321%) than the theoretical values of Δp, calculated according to the standard [49] with the absolute roughness of the internal pipeline wall assumed as k = 4 mm.

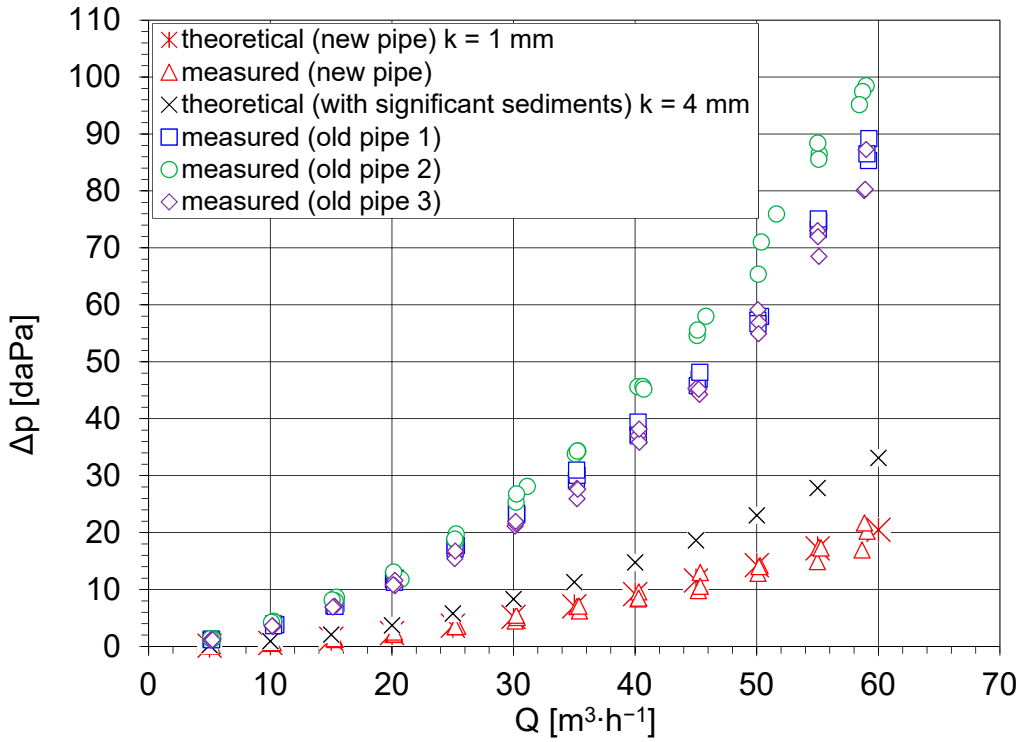

Figure 3. Pressure difference Δp calculated for the cast-iron pipes with the internal diameter d = 150 mm according to the standard [49] and measured for the new pipe and pipes after 30-year exploitation.

Table 2. Absolute roughness coefficient k for cast-iron pipes [49].

Surface state and Exploitation Conditions	Roughness k 10^{-3} [m]
New	0.25–1.0
new, bituminized	0.10–0.15
Asphalted	0.12–0.30
water pipes in exploitation	1.4
pipes in exploitation, corroded	1.0–1.5
with sediments	1.0–1.5
with considerable sediments	2.0–4.0
purified after several years of exploitation	0.3–1.5
severely corroded	≤3.0

Using the derived Equation (8) for the assumed values of water flow rate Q and measured real values of the pressure difference Δp in the individual pipes (Figure 3), the absolute roughnesses k of the internal pipeline wall for the new pipe and pipes after 30-year exploitation were calculated and presented in Figure 4 as a function of the Reynolds number Re. The Reynolds number depends on the water volume flow velocity, pipe internal diameter and water kinematic viscosity coefficient, thus very well describes the water hydraulic flow conditions in the investigated pipes; therefore, researchers analyze the roughness of internal pipe walls as a function of the Reynolds number [59–61].

The determined values of the absolute roughness k of the internal pipe wall are not constant, but they decrease as the Reynolds number increases till $Re = 6 \cdot 10^4$ (Figure 4). After exceeding this value, the determined absolute roughness of the internal pipe wall is stable and for the investigated pipes after 30-year exploitation equal to k = 27.6 mm (0.92 mm/yr) on average (for the pipes: nr 1—25.9 mm (0.86 mm/yr); nr 2—32.7 mm (1.09 mm/yr); nr 3—24.2 mm (0.81 mm/yr)). Other authors also provide significant increments of pipe roughness after a long-year exploitation. For example, Annus and Vassiljev [17] informed

that after 41 years of exploitation the roughness was equal to 36 mm, (0.86 mm/yr). Other researchers provide even higher increments, at a level of 2.13 mm/yr [15]. Theoretical values of roughness calculated according to the formulas given by Shahzad and James [58] and Pelka [14] for cast-iron pipes after 30-year exploitation fluctuate within the range of 2.55 mm to 5.08 mm. On this basis, it can be concluded that the values of roughness determined according to the formulas provided in the literature can be underestimated.

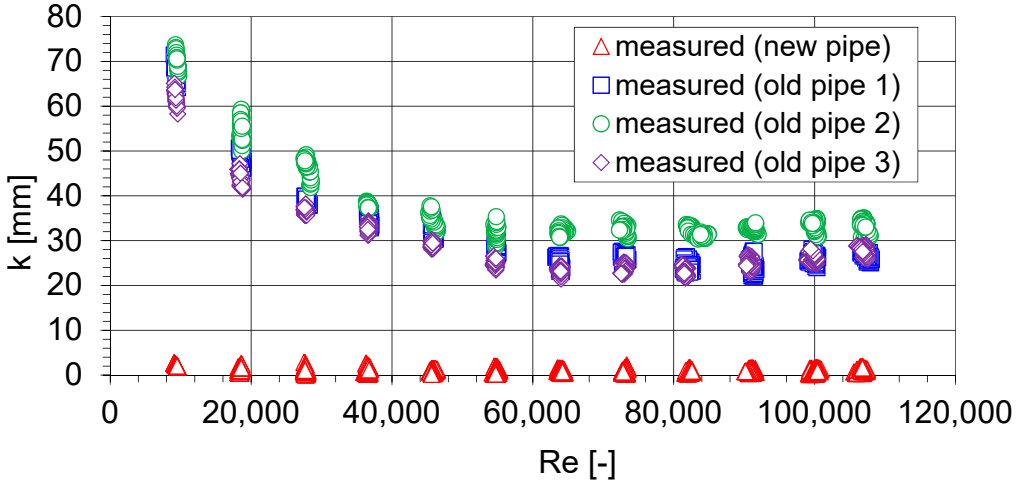

Figure 4. Absolute roughness k of the internal walls of the cast-iron pipelines with the internal diameter d = 150 mm, calculated according to Formula (8) for the new pipe and pipes after 30-year exploitation.

According to Formula (9), the equivalent internal diameter d_t after 30-year exploitation for the pipes being investigated is equal to 94.8 mm on average (for the pipes: nr 1—98.2 mm, nr 2—84.6 mm, nr 3—101.6 mm).

For the new pipe, however, and for the whole range of the Reynolds number, the determined value of the absolute roughness of the internal pipe wall is stable and equal to k = 0.9 mm on average. The accumulated sediment in the pipes after 30-year exploitation evoked 30-fold increase of the absolute roughness, if compared to the new pipeline. The results of measurements of the pressure difference Δp (Figure 3) and results of calculations of the absolute roughness of the internal pipe wall k (Figure 4) show that the classical formulas for calculation of major head losses (pressure difference Δp) should not be applied for the exploited pipes with considerable sediments because they do not allow to obtain comparable (stable) values of the absolute roughness k of the internal pipe wall in the whole range of the analyzed Reynolds number.

Investigations of roughness of the sediment accumulated in the water supply pipelines after 30-year exploitation were performed with use of the Hirox KH-8700 digital microscope (Hirox, Tokyo, Japan). Sediment roughness measurement—linear and superficial—was made for selected fragments of the investigated pipes. The results are characterized by high variability, depending on a tested sample. For the analyzed pipes, very high spatial variability of forms of sediments accumulated in the pipes prevented from fixing reliable indicators of their roughness. An example distribution of the roughness of the sediment surface for the investigated pipes is presented in Figure 5. Digital microscopes can be applied for empirical measurements of the sediment roughness, especially in the presence of more homogeneous distribution of the roughness at the internal pipe wall.

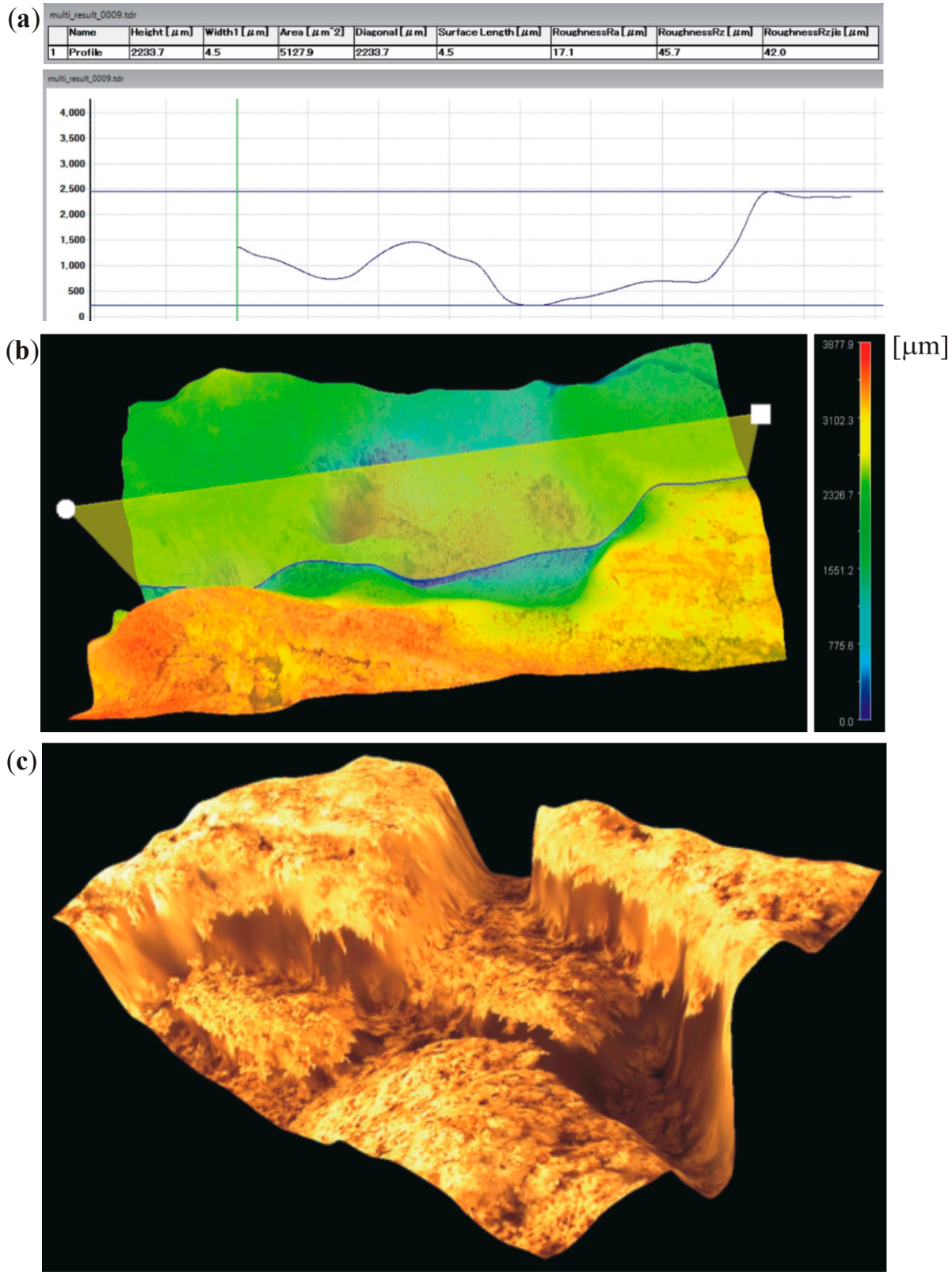

Figure 5. Results of measurement of sediment surface roughness with the use of the HIROX RH-8700 digital microscope: (**a**) table with results of measurement of sediment surface roughness and longitudinal profile of the investigated sediment surface; (**b**) spatial visualization of longitudinal profile of the investigated sediment surface; (**c**) 3-dimensional visualization of the investigated sediment surface.

Investigations of structure and chemical composition of the sediments accumulated in the analyzed water supply pipelines were performed as well. The mineral composition was determined with the use of the X-ray phase analysis (XRD) and is presented in Figure 6. It is dominated by the ferric oxyhydroxides represented by goethite (α-FeOOH) and lepidocrocite (γ-FeOOH), accompanied by gypsum and sulfur. The goethite was identified by the strongest and characteristic interplanar distances d_{hkl} = 4.184; 2.693; 2.488; 2.451 Å. The lepidocrocite was identified by the distances d_{hkl} = 6.250; 3.289; 2.469; 1.938 Å. Apart from the ferric oxyhydroxides, there was calcium sulfate—gypsum ($CaSO_4 \cdot 2H_2O$) in the sediment; it was identified by the strongest interplanar distances d_{hkl} = 7.634; 4.292; 3.067; 2.874 Å. The mineral composition of the sediment is completed by the sulfur. This phase was identified by the strongest interplanar distances d_{hkl} = 3.846; 3.436; 3.333; 3.205 Å.

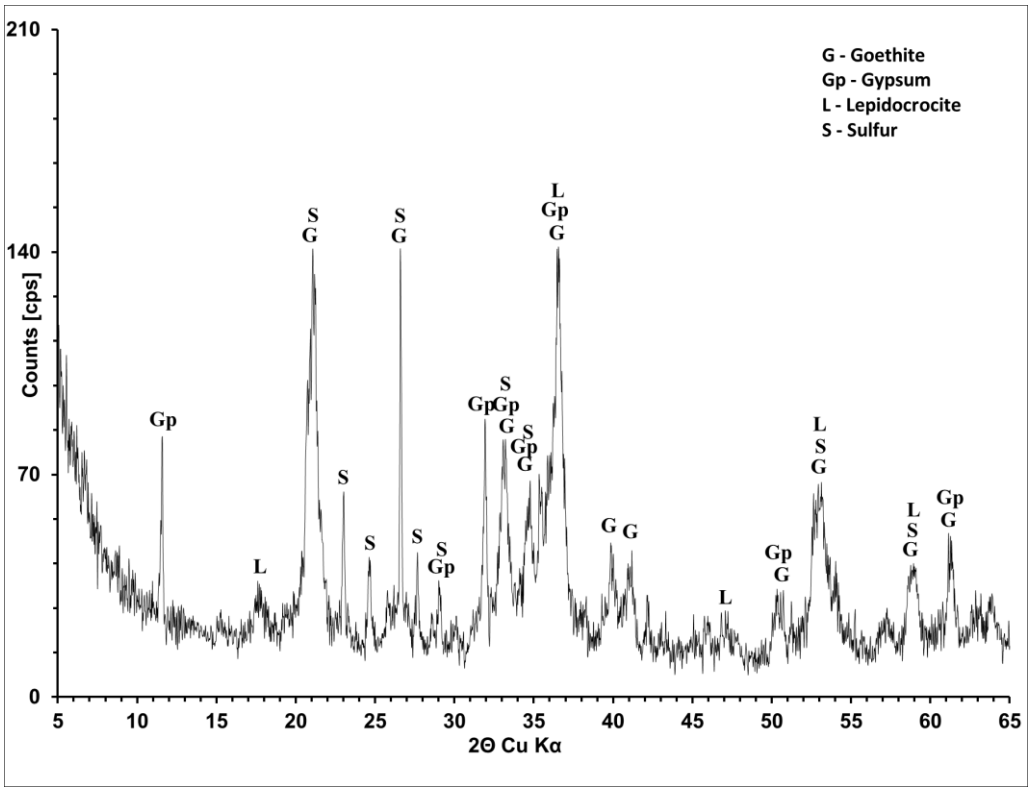

Figure 6. Diffraction pattern of the sediment mineral composition.

The image of the sediments at the 35× magnification is presented in Figure 7. Basing on a visual evaluation, one can state that the sediments are yellow-brown, which can prove that the iron oxides dominate there. The surface of the sediments is irregular, flat areas and distinct local hollows occur. One can observe sediments characterized by strong solidification as well as loosely solidified sediments, which assume a powdery or dusty form as they go dry.

Figure 8a presents microstructure of the sediments in the external zone. In the scanning microscope image, thin tile-shaped aggregates of iron oxides / hydroxides are visible. These aggregates represent two morphological forms: (I)—tile-shaped, mutually superimposed conglomerates with a porous structure (point 1); (II)—radiant conglomerates consisting of crystallites lying around a common centre of compact structure (point 2). Their chemical composition is very similar, the iron dominates, accompanied by small contents of S, Ca and Cl, which is proven by the EDS spectra (Figure 8b).

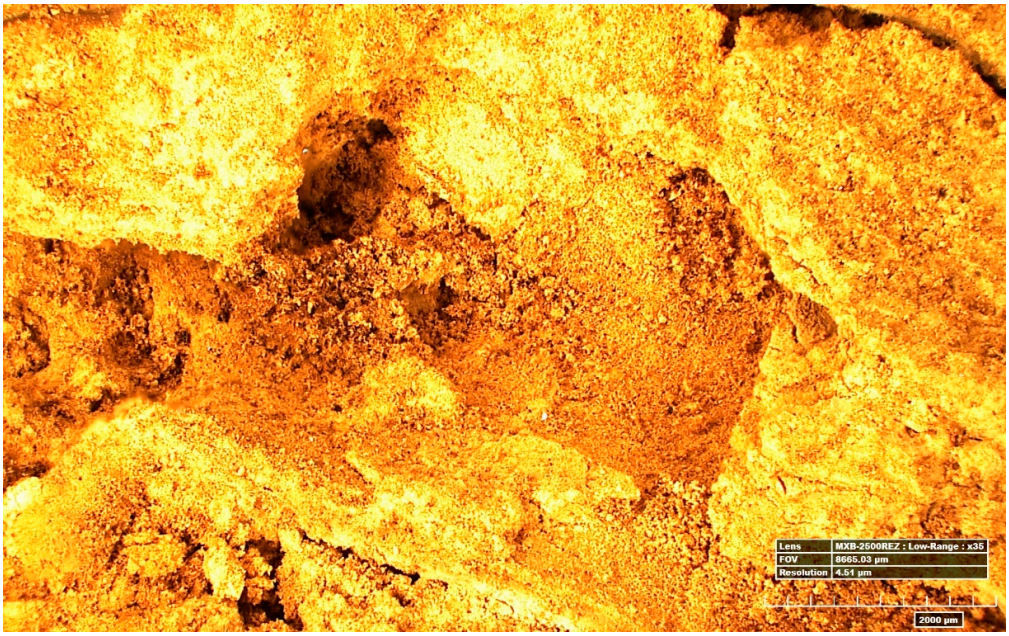

Figure 7. Image of sediment surface obtained in the HIROX RH-8700 digital microscope (magnification 35×).

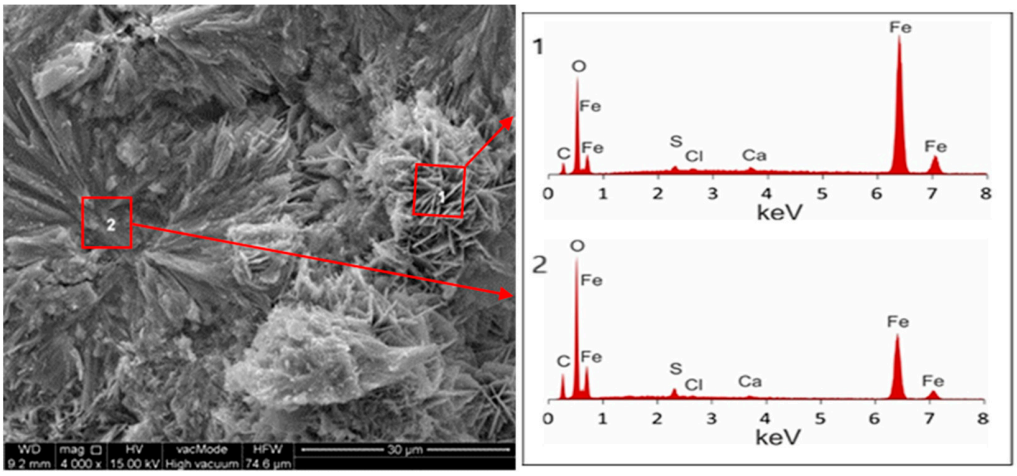

(**a**) (**b**)

Figure 8. Morphology of the outer layer of the sediment on a corroded cast-iron pipe: (**a**) SEM micrograph; (**b**) spectrum of chemical composition (EDS) of the sediment in points 1 and 2.

The inner layer of the sediment on the corroded cast-iron pipe represents a different type of microstructure (Figure 9a). Compact, massive aggregates consisting of the calcium carbonate (calcite—$CaCO_3$) dominate, sometimes with a distinct 3-directional cleavage (point 1), accompanied by microareas with a porous structure having the nature of a corrosion. Fine-grained aggregates of crystals, occurring in this zone, are non-homogeneous and characterized by a chemical composition where, apart from CA, significant quantities of Fe and S as well as trace quantities of Cl occur. The differences in the chemical composition are shown in Figure 9b.

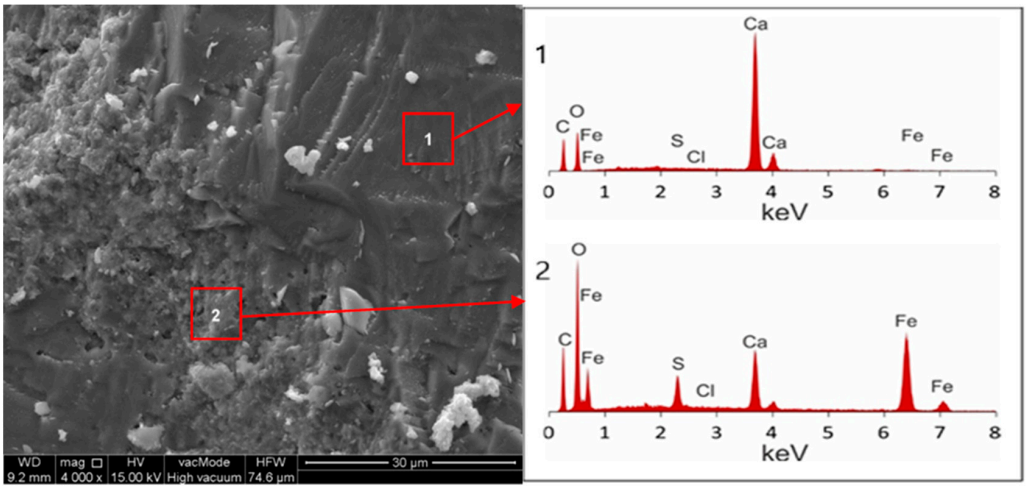

(a) **(b)**

Figure 9. Morphology of the outer layer of the sediment on a corroded cast-iron pipe: (**a**) SEM micrograph; (**b**) spectrum of chemical composition (EDS) of the sediment in points 1 and 2.

In the accumulated sediments, the iron oxides dominate in the outer layer, whereas the calcium oxides or iron oxides—in the internal layer (Table 3). Both in the outer layer and inner layer, the sulfates and dichlorine monoxide occur.

Table 3. Chemical composition of the sediment in the outer layer and inner layer.

Tested Substance	Outer Layer				Inner Layer			
	1	1	2	2	1	1	2	2
SO_3	1.11	2.14	5.55	10.26	0.38	0.27	8.77	12.87
Cl_2O	0.38	0.69	0.54	0.92	0.26	0.17	0.17	0.23
CaO	0.85	2.35	1.07	2.84	97.35	98.84	14.65	30.70
Fe_2O_3	97.66	94.81	92.83	85.99	2.01	0.72	76.40	56.20

The investigations with use of XRF showed that the dominating component of the accumulated sediments are the iron oxides (Table 4).

Table 4. Sediment XRF tests.

Component	Na_2O	MgO	Al_2O_3	SiO_2	P_2O_5	SO_3	K_2O	CaO	TiO_2	Fe_2O_3
%	0	0	0.17	2.07	0.44	1.19	0	0.23	0.02	94.06

The calculated Langelier saturation index for the water flowing in the analyzed pipelines was equal to 0.07 and the Ryznar index—7.1

4. Discussion

Figure 10 presents average values of real pressure difference Δp, i.e., hydraulic losses, obtained in measurements and calculations for the cast-iron pipes with the internal diameter d = 150 mm as a function of water flow rate Q. During the measurements and calculations, the hydraulic losses in the pipes increased along with the increase of water flow rate (Figure 10) and this trend is concordant with the literature data [27,62]. The lowest hydraulic losses during the water flow occurred in the new pipe, the highest—in the pipe after 30-year exploitation. The trend (regression) type of the measured and calculated values of Δp was exponential and values of coefficients of determination (R^2) from the sample were equal to 1, which indicates that the hydraulic losses in the cast-iron pipes in

100% depend on the water flow rate Q and absolute roughness k of the internal pipeline wall. The remaining factors, such as the water temperature or gravitational acceleration, do not affect significantly the average values of pressure difference Δp.

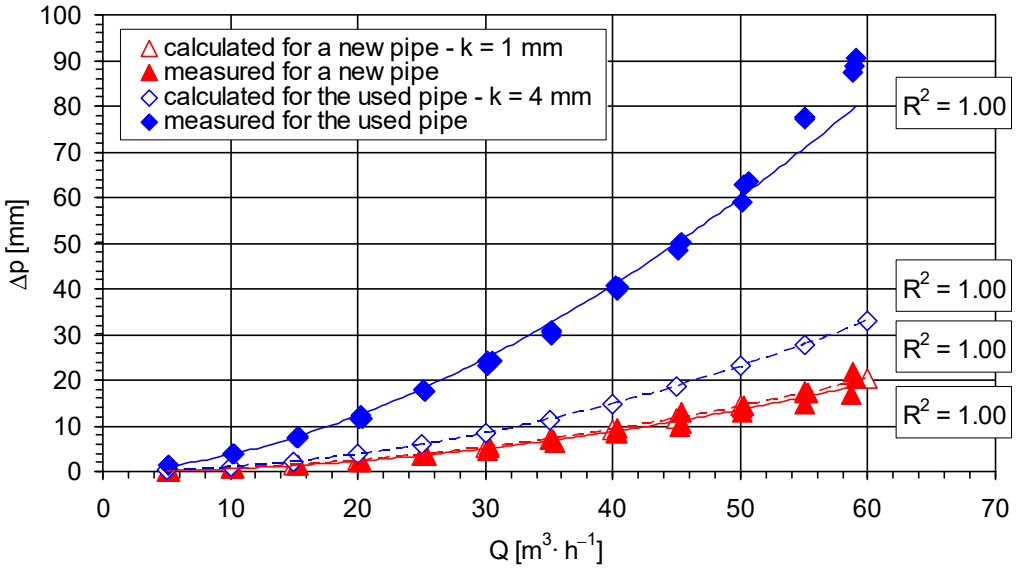

Figure 10. Average values of real pressure difference Δp calculated for the cast-iron pipes with the internal diameter d = 150 mm according to the standard [49] and measured for the new pipe and for the pipes after 30-year exploitation.

Figure 11 presents average values of the absolute roughness k of the internal pipeline wall, calculated for the cast-iron pipes with the internal diameter d = 50 mm according Equation (8) as a function of the Reynolds number Re. As the Reynolds number grew, the average values of the absolute roughness k initially decreased and then assumed constant values (Figure 11); this trend is concordant with the literature data [15,45,63]. The lowest values of the absolute roughness occurred in the new pipe and the highest—in the pipe after 30-year exploitation. The trend (regression) type of the determined values of k was of a 6th order polynomial and values of coefficients of determination (R^2) from the sample were higher than 0.67, which indicates that the absolute roughness k of the internal pipeline wall at least in 67% depends on the Reynolds number Re, i.e., water flow velocity V, pipe diameter d and water kinematic viscosity coefficient ν, as well as the pipe exploitation period, whereas in 33% it depends on the pressure difference Δp existing in the pipe during the water flow.

A statistical analysis was also carried out in aim to check whether the differences of average values in the results concerning the absolute roughness k for the analysed pipes (Figure 11) are statistically significant. The statistical analysis was performed for the results obtained for the Reynolds number $Re > 6 \cdot 10^4$. At first, the normality of distribution was checked using the Shapiro–Wilk test and then the homogeneity of variance with use of the Levene test. In both tests for individual groups, the values of calculated probability p_{cal} were greater than the assumed significance level $\alpha = 0.05$, which means that the conditions of normal distribution and homogeneity of variance in the examined groups are satisfied. Calculations of the distribution normality and variance homogeneity were made with use of the *Statistica* software. Then, the Student's t-test was applied for two populations: according to the zero hypothesis (H_0: $n_1 = n_2$), the differences between the average values are statistically equal to each other, and according to the alternative hypothesis (H_1: $n_1 \neq n_2$), these differences are statistically different. Calculations of the value of Student's t-statistics $|t_{cal}|$ were performed with use of the *Statistica* program and the obtained results are shown in Table 5.

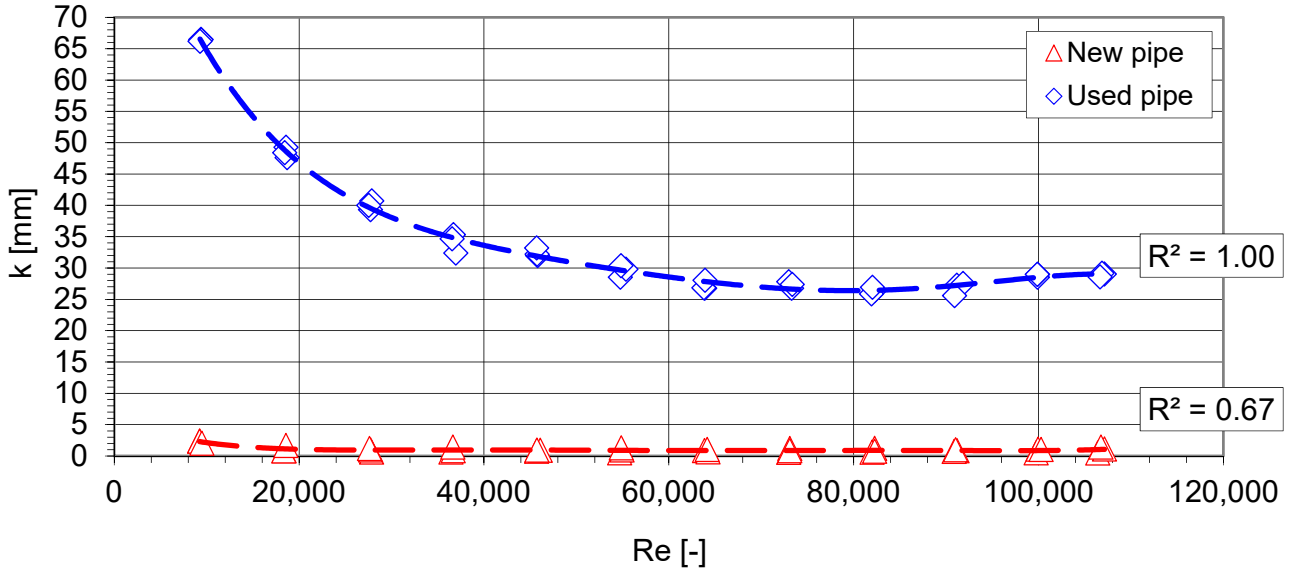

Figure 11. Average values of absolute roughness k of the internal pipeline wall calculated for the cast-iron pipes with the internal diameter d = 150 mm according to Equation (8) for the new pipe and the pipes after 30-year exploitation.

Table 5. Results of calculations of the Student's t-statistics. The differences of average values are significant with probability $p < 0.05$.

Type of the Pipe	Mean Value	Standard Deviation	Obtained Student's t-test Value $\lvert t_{cal} \rvert$	Obtained Probability Value p_{cal}	Student's t-statistics Value Read from the Tables for p = 0.05 and v = 34 $t_{\alpha = 0.05}$
New pipe	0.899	0.266	−99.726	$5.668 \cdot 10^{-25}$	2.101 *
Exploited pipe	27.593	1.126			

* value read from statistical tables [64].

For the alternative hypothesis, a critical area $\lvert t_{cal} \rvert \geq t_{\alpha=0.05}$ was determined and then for $v = n_1 + n_2 - 2 = 34$ degrees of freedom and $\alpha = 0.05$ (the assumed 5-percentage risk of error, i.e., significance level) a critical value $t_{\alpha=0.05} = 2.101$ was read from the tables of the Student's t-distribution. Table 5 shows that $\lvert t_{cal} \rvert \geq t_{\alpha=0.05}$, thus the zero hypothesis must be rejected and it can be concluded that the differences of average values in the results concerning the absolute roughness k for the analyzed pipes are indeed statistically significant. It is also confirmed by the calculated probability value—p_{cal} is lower than 0.05 (assumed significance level).

The flowability drop coefficient η_t of a pipeline defines a ratio between flow rate in a pipeline after t years of exploitation and in a new pipeline, at the same pressure line slope. The flowability drop coefficient for the investigated pipes and calculated by other researchers [43,44,65] is presented in Figure 12. Kamersztein classified waters into five groups depending on corrosive features and precipitatibility: group 1 contains non-corrosive waters with low precipitatibility and group 5—highly corrosive waters with high carbonate hardness.

The measured flowability drop coefficient for the pipe after 30-year exploitation is lower than the coefficient calculated according to the formulas submitted by Barnes [65] and Khatib [43], as well as Kamersztein [44] for slightly corrosive waters. This coefficient should be 0.54 according to Barnes, 0.6—to Khatib, 0.76—to Kamersztein. The flowability drop coefficient for the investigated pipes fluctuated between 0.36 and 0.52, and it was equal to 0.45 on average.

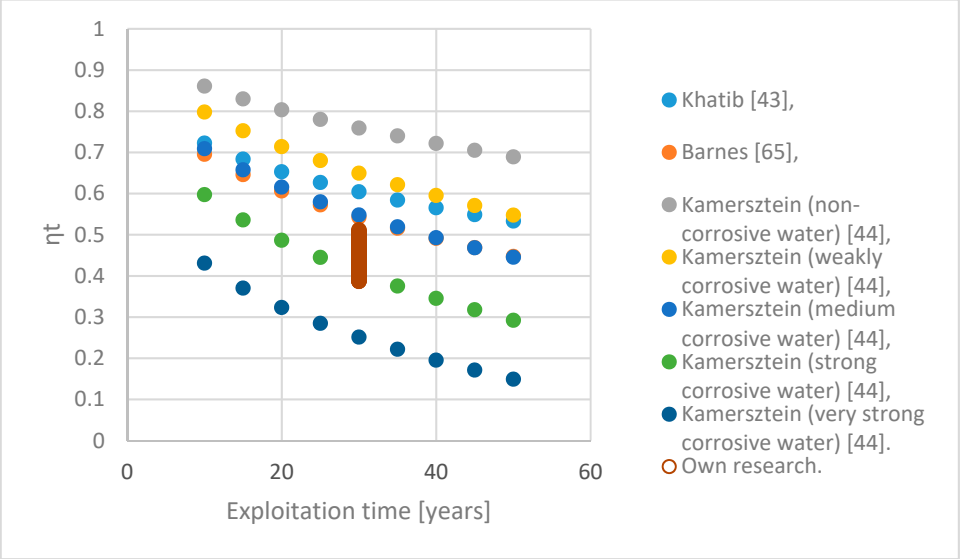

Figure 12. Flowability drop of the investigated pipes after 30-year exploitation, compared to the literature data.

The flowability reduction increases the pressure losses and affects the flow velocity through the pipes, but this reduction in the pipe diameter is usually ignored. Exact estimation of the diameter reduction is very complicated [66]. There are usually two approaches in the case of changes of the diameter. The first one is neglection of the reduction of pipe diameter. This assumption is popular mainly in simulations of hydraulic models (Aquis). It is assumed here that in aim to assess the roughness increase, the diameter reduction has been already taken into account in the concept because the roughness magnitude is being estimated with consideration of the influence of a pipe material and water quality. Secondly, the flowability decrease must be predicted by a separate estimation of a roughness and diameter and then the pressure loss is being calculated as a result of both of them. With this assumption, the pipe roughness increase and the diameter reduction is calculated separately, though they can mutually affect each other [67]. In the paper, the flowability reduction for the pipes being investigated was calculated based on the roughness increase.

Pipe material, water quality and reaction of the material to a contact with water have a direct impact on the diameter reduction. This reduction is a result of chemical and physical processes inside the pipes, such as sedimentation, encrustation, fouling and corrosion [58]. The performed investigations of the sediment structure indicate its diversification (Figures 8 and 9). In the outer layer, irregular or radiant tile-shaped conglomerates were observed. The chemical composition is dominated by Fe, accompanied by small quantities of S, Ca and Cl. The internal layer of the sediment is dominated by compact aggregates accompanied by microareas with a porous structure. In this layer, apart of Ca, significant quantities of Fe and S and trace quantities of Cl occur. They are typical components of sediments accumulating in water supply systems using waters from underground sources and largely result from a chemical composition of the transported water. The iron in underground waters is found naturally and it is partially removed in conditioning processes. As a result of aeration, the iron ions precipitate from water in the form of iron oxides and hydroxides. The content of calcium and magnesium ions in water can be diversified and affects its hardness and ability to precipitate sediments in the form of calcium and magnesium carbonates. Sulfates in water are usually found naturally and affect precipitation of indissoluble sulfides. The presence of the dichlorine monoxide in sediments can result from temporary disinfection of water supply network. Frequently chemicals containing chlorine are used to this aim, e.g., sodium hypochlorite.

If the Langelier saturation index LSI > 0, then water tends to precipitate sediments and corrosive features of water are weakened. If LSI = 0, then the water does not tend to precipitate sediments and its corrosive features are also weakened. If LSI < 0, then the water does not tend to precipitate sediments and its corrosive features are strengthened [68]. In relation to the LSI, the Ryznar stability index broadens the range of parameters liable to affect corrosion and water hardness because it considers magnesium content, temperature and dry residue, which indirectly considers typical components of dissolved substances, i.e., chlorides and sulfides. The RSI has a more extended corrosivity range than the LSI: 4 < RSI < 5—strong precipitation of sediment, 5 < RSI < 6—medium precipitation of sediment, 6 < RSI < 7—weak precipitation of sediment or initial corrosion, 7 < RSI < 7.5—corrosion, 7.5 < RSI < 9—strong corrosion, RSI > 9—very strong corrosion [56,57,68–71]. Basing on the performed determinations of quality parameters of the water transported by the investigated cast-iron pipelines (Table 1), the Langelier saturation index was calculated, which amounted to 0.07, which indicates very low precipitatibility, whereas the Ryznar index amounted to 7.17, which indicates very low corrosive features of the water flowing through the investigated pipelines. In the case under consideration, significant accumulation of sediments was stated, although the water flowing through the investigated pipelines presented very low or no corrosive features and precipitatibility.

5. Conclusions

For the investigated cast-iron pipes, a pitting corrosion, wall thickness reduction and wall degradation were not observed, which proves that the destruction of the pipes was not significant and it is possible to prolong their life. Evaluation of the corrosivity of the buried cast-iron pipes, exploited for 30 years in the potable water supply system, confirmed high durability and long life of the cast-iron pipes. Significant quantities of sediments precipitating inside the pipes, however, revealed to be a problem, although the water being distributed through the investigated pipelines, according to the calculated Langelier and Ryzner indexes, presented very low or no corrosive features and precipitatibility.

Big quantities of precipitation evoke significant deterioration of hydraulic flow conditions. The measured pressure losses in the pipes after 30-year exploitation are five times higher on average (502%) than the measured real values of the pressure difference for the new pipe and over threefold higher on average (321%) than the theoretical values for pipes with significant sediments [49]. The flowability drop coefficient for the investigated pipes fluctuated between 0.36 and 0.52 and, on average, it was equal to 0.45. It means that after 30-year exploitation, 45% of flow rate generates the same pressure losses as in new pipes. The performed investigations showed that the transport of water through the investigated pipes involves significant energy losses because the average absolute roughness (k = 27.6 mm) grew threefold if compared to the new pipeline; therefore, its further exploitation can be economically unjust. In such situation, it should be considered its exchange or, having in mind a good technical state of the pipe wall, a possibility of removing the accumulated sediments from the pipeline and securing its internal surface against re-accumulation of sediments.

The structure and chemical composition of the accumulated sediments are diversified in the outer and inner layers. The chemical composition of the accumulated sediments, both in the outer and inner layers, is dominated by iron oxides and hydroxides. In the internal layer, higher content of calcium is observed. Significant accumulation of sediments in the investigated pipes can lead to re-deterioration of quality and to the so-called red water effect.

Author Contributions: Conceptualization, P.W., M.K. and D.M.; methodology, P.W., M.K., D.M. and A.L.; investigation, P.W., M.K., D.M. and A.L.; data curation, P.W. and M.K.; writing—original draft preparation, P.W.; writing—review and editing, M.K., A.L. and M.C.; visualization, P.W., M.K. and M.C.; supervision, P.W.; All authors have read and agreed to the published version of the manuscript.

Funding: This research received no external funding.

Institutional Review Board Statement: Not applicable.

Informed Consent Statement: Not applicable.

Data Availability Statement: The data presented in this study is available on request from the corresponding author.

Conflicts of Interest: The authors declare no conflict of interest.

References

1. Wichowski, P.; Rutkowska, G.; Kamiński, N.; Trach, Y. Analysis of water consumption in the campus of Warsaw University of Life Sciences in years 2012–2016. *J. Ecol. Eng.* **2019**, *20*, 193–202. [CrossRef]
2. *Safe Piped Water Managing Microbial Water Quality in Piped Distribution Systems*; Richard, A. (Ed.) IWA Publishing: London, UK, 2004.
3. *Guidelines for Drinking-water Quality: Incorporating 1st and 2nd Addenda*, 3rd ed.; World Health Organization: Geneva, Switzerland, 2008; Volume 1, ISBN 978 92 4 154761 1. Available online: https://www.who.int/water_sanitation_health/dwq/fulltext.pdf (accessed on 22 March 2021).
4. U.S. Environmental Protection Agency (EPA). *Water Quality Standards Handbook: Chapter 3: Water Quality Criteria*; EPA-823-B-17-001; EPA: Washington, DC, USA, 2017. Available online: https://www.epa.gov/sites/production/files/2014-10/documents/handbook-chapter3.pdf (accessed on 22 March 2021).
5. Guidelines for Drinking-Water Quality. *Guidelines for Drinking-Water Quality: Incorporating First Addendum*, 3rd ed.; World Health Organization: Geneva, Switzerland, 2020; Volume 1. Available online: https://www.who.int/water_sanitation_health/dwq/gdwq0506.pdf (accessed on 22 March 2021).
6. Hu, J.; Dong, H.; Xu, Q.; Ling, W.; Qu, J.; Qiang, Z. Impacts of water quality on the corrosion of cast iron pipes for water distribution and proposed source water switch strategy. *Water Res.* **2018**, *129*, 428–435. [CrossRef]
7. Ravi Shankar, A.; Anandkumar, B.; Thinaharan, C.; George, R.P.; Rooby, J.; Philip, J.; Kamachi Mudali, U. Corrosion Evaluation of Buried Cast Iron Pipes Exposed to Fire Water System for 30 years. *Trans. Indian Inst. Met.* **2020**, *73*, 9–21. [CrossRef]
8. Beech, I.B.; Sunner, J. Biocorrosion: Towards understanding interactions between biofilms and metals. *Curr. Opin. Biotechnol.* **2004**, *15*, 181–186. [CrossRef]
9. Teng, F.; Guan, Y.T.; Zhu, W.P. Effect of biofilm on cast iron pipe corrosion in drinking water distribution system: Corrosion scales characterization and microbial community structure investigation. *Corros. Sci.* **2008**, *50*, 2816–2823. [CrossRef]
10. Usher, K.M.; Kaksonen, A.H.; Cole, I.; Marney, D. Critical review: Microbially influenced corrosion of buried carbonsteel pipes. *Int. Biodeterior. Biodegrad.* **2014**, *93*, 84–106. [CrossRef]
11. Xu, D.; Li, Y.; Gu, T. Mechanistic modeling of biocorrosion caused by biofilms of sulfatereducing bacteria and acid producing bacteria. *Bioelectrochemistry* **2016**, *110*, 52–58. [CrossRef]
12. Liu, G.; Zhang, Y.; Knibbe, W.J.; Feng, C.; Liu, W.; Medema, G.; van der Meer, W. Potential impacts of changing supply-water quality on drinking water distribution: A review. *Water Res.* **2017**, *116*, 135–148. [CrossRef]
13. Li, M.; Liu, Z.; Chen, Y. Physico-chemical Characteristics of Corrosion Scales from Different Pipes in Drinking Water Distribution Systems. *Water* **2018**, *10*, 931. [CrossRef]
14. Pelka, H. On the effect of some chemical properties of water on the hydraulic resistance of pipes. *Ochr. Sr.* **1985**, *2–3*, 19–24.
15. Echavez, G. Increase in losses coefficient with age for small diameter pipes. *J. Hydraul. Eng.* **1997**, *2*, 157–159. [CrossRef]
16. Siwoń, Z.; Cieżak, J.; Bogaczewicz, S. On the Increase of Hydraulic Resistance in Cast Iron and Steel Pipes of the Water Supply Network for the City of Wrocław. *Ochr. Sr.* **1998**, *20*(4), 21–26.
17. Annus, I.; Vassiljev, A. Different approaches for calibration of an operational water distribution system containing old pipes. *Procedia Eng.* **2015**, *119*, 526–534. [CrossRef]
18. McNeill, L.S.; Edwards, M. Iron pipe corrosion in distribution systems. *J. Am. Water Work. Assoc.* **2001**, *93*, 88–100. [CrossRef]
19. Rajeev, P.; Kodikara, J.; Robert, D.; Zeman, P.; Rajani, B. Factors contributing to large diameter water pipe failure. *Water Asset. Manage. Int.* **2014**, *10*, 9–14.
20. U.S. Environmental Protection Agency (EPA). *2006 Community Water System Survey. EPA 815-R-09-001*; US Environmental Protection Agency: Washington, DC, USA, 2009. Available online: https://nepis.epa.gov/Exe/ZyPDF.cgi?Dockey=P1009JJI.txt (accessed on 24 January 2021).
21. AWWA. *Buried No Longer: Confronting America's Water Infrastructure Challenge*; American Water Works Association Research Foundation: Denver, CO, USA, 2011.
22. Grigg, N.S. *Secondary Impacts of Corrosion Control on Distribution System and Treatment Plant Equipment*; Water Research Foundation: Denver, CO, USA, 2010.
23. Philibert, M.; Mendaza, S.; Zraick, F.; Rabaud, B. Predicting the effect of water quality on water distribution cast iron and steel pipes using two novel indices. *Sci. Technol. Water Suppl.* **2018**, *18*, 524–538.
24. Lewicki, Z. Calculation of hydraulic losses in pipes of water supply networks. (Obliczanie strat hydraulicznych w przewodach czynnych sieci wodociągowych). University of Science and Technology in Zielona Góra. *Sci. Issues* **1978**, *51*, 65–82. (In Polish).
25. Mielcarzewicz, E.W. *Calculation of Water Supply Systems. (Obliczanie Systemów Zaopatrzenia w Wodę)*; GWF: Arkady, Warsaw, Poland, 2000; pp. 47–69. (In Polish)

26. Colebrook, C.F.; White, C.M. Experiments with fluid friction in roughened pipes. *Proc. R. Soc. A Math. Phys. Eng. Sci* **1937**, *161*, 367–381.
27. Shashi Menon, E. *Transmission Pipeline Calculations and Simulations Manual*, 1st ed.; Gulf Professional Publishing; Elsevier Inc.: Amsterdam, The Netherlands, 2015; p. 612.
28. Malcolm, J.; Brandt, K.; Johnson, M.; Elphinston, A.J.; Ratnayaka, D.D. *Twort's Water Supply*, 7th ed.; Elsevier Ltd.: Amsterdam, The Netherlands, 2017; pp. 581–619.
29. Brkić, D. Review of explicit approximations to the Colebrook relation for flow friction. *J. Pet. Sci. Eng.* **2011**, *77*, 34–48. [CrossRef]
30. Brkić, D. A note on explicit approximations to Colebrooks friction factor in rough pipes under highly turbulent cases. *Int. J. Heat Mass Transf.* **2016**, *93*, 513–515. [CrossRef]
31. Kalenik, M. Empirical Formulas for Calculation of Negative Pressure Difference in Vacuum Pipelines. *Water* **2015**, *7*, 5284–5304. [CrossRef]
32. Kalenik, M. Real Values of Local Resistance Coefficient During Flow of Water Through Welded Polypropylene Elbows. *Ochr. Sr.* **2019**, *41*, 23–30.
33. Wichowski, P.; Siwiec, T.; Kalenik, M. Effect of the Concentration of Sand in a Mixture of Water and Sand Flowing through PP and PVC Elbows on the Minor Head Loss Coefficient. *Water* **2019**, *11*, 828. [CrossRef]
34. Kalenik, M.; Chalecki, M.; Wichowski, P. Real Values of Local Resistance Coefficients during Water Flow through Welded Polypropylene T-Junctions. *Water* **2020**, *12*, 895. [CrossRef]
35. Ono, A.; Kimura, N.; Kamide, H.; Tobita, A. Influence of elbow curvature on flow structure at elbow outlet under high Reynolds number condition. *Nucl. Eng. Des.* **2011**, *41*, 4409–4419. [CrossRef]
36. Csizmadia, P.; Hős, C. CFD-based estimation and experiments on the loss coefficient for Bingham and power-law fluids through diffusers and elbows. *Comp. Fluids* **2014**, *99*, 116–123. [CrossRef]
37. Dutta, P.; Nandi, N. Effect of Reynolds number and curvature ratio on single phase turbulent flow in pipe bends. *Mech. Mech. Eng.* **2015**, *19*, 5–16.
38. Dutta, P.; Saha, S.K.; Nandi, N.; Pal, N. Numerical study on flow separation in 90° pipe bend under high Reynolds number by k-ε modelling. *Int. J. Eng. Sci. Technol.* **2016**, *19*, 904–910. [CrossRef]
39. Chowdhury, R.R.; Alam, M.M.; Sadrul Islam, A.K.M. Numerical modeling of turbulent flow through bend pipes. *Mech. Eng. Res. J.* **2016**, *10*, 14–19.
40. Colebrook, C.F.; White, C.M. The reduction of currying capacity of pipes with age. *J. Civ. Eng.* **1937**, *1*, 99–118.
41. Mohebbi, H.; Li, C.Q. Experimental Investigation on Corrosion of Cast Iron Pipes. *Int. J. Corros.* **2011**, *2011*, 1–17. [CrossRef]
42. Korte, J.W.; Bodarwe, H. *Eine Grundsätzliche Gesichtspunkte zur Berechnung von Wasserversorgungsnetzen*; GWF: Essen, Germany, 1958; pp. 117–1184.
43. Khatib, A. Research on hydraulic efficiency of water pipes. Ph.D. thesis, University of Technology, Wroclaw, Poland, 1992.
44. Kamersztejn, A.G. *Mieroprijatija po Sochranieniju Propusknoj Sposobnosti Wodoprowodnych Trub*; GWF: Strojizdat, Moscow, Russia, 1950.
45. Malesinska, A.; Chudzicki, J. Change in Hydraulic Resistance of Water Supply Pipes Being Renovated with Polyethylene Pipes. *Ochr. Sr.* **2014**, *36*, 29–35.
46. Abdel-Monim, Y.K.; Ead, S.A.; Shabayek, S.A. Effect of time on pipe roughness. 17th Canadian Hydrotechnical Conference. *CSCE* **2005**, *2005*, 1–10.
47. Kandlikar, S.G.; Schmitt, D.; Carrano, A.L.; Taylor, J.B. Characterization of surface roughness effects on pressure drop in singlephase flow in minichannels. *Phys. Fluids* **2005**, *17*, 10. [CrossRef]
48. DIN 19210:1984. *Methods for Measurement of Fluid Flow—Differential Pressure Piping for Flow Measurement Devices*; German standard DIN 19210; Deutsches Institut fur Normung E.V. (DIN): Berlin, Germany, Volume 1984; pp. 1–6.
49. PN-76 M-34034:1976. *Principles of Calculating Pressure Losses*; Polish standard PN-76 M-34034; Polish Committee for Standardization: Warsaw, Poland, 1976; pp. 1–25.
50. *Corrosion Manual for Internal Corrosion of Water Distribution Systems*; United States Environmental Protection Agency: Washington, DC, USA, 1984.
51. Melidis, P.; Sanosidou, M.; Mandusa, A.; Ouzounis, K. Corrosion control by using indirect methods. *Desalination* **2007**, *213*, 152–158. [CrossRef]
52. Amouei, A.; Fallah, H.; Asgharnia, H.; Bour, R.; Mehdinia, M. Evaluation of corrosion and scaling potential of drinking waterresources in Noor city (Iran) by using stability indice. *Koomesh* **2016**, *18*, 326–333.
53. Abbasnia, A.; Alimohammadi, M.; Mahvi, A.H.; Nabizadeh, R.; Yousefi, M.; Mohammadi, A.A.; Pasalari, H.; Mirzabeigi, M. Assessment of groundwater quality and evaluation of scaling and corrosiveness potential of drinking water samples in villages of Chabahr city, Sistan and Baluchistan province in Iran. *Data Brief* **2018**, *16*, 182–192. [CrossRef] [PubMed]
54. Langelier, W.F. The analytical control of anti-corrosion water treatment. *J. Am. Water Works Assoc.* **1936**, *28*, 1500–1521. [CrossRef]
55. Ryznar, J.W. A new index for determining the amount of calcium carbonate scale formed by water. *J. Am. Water Works Assoc.* **1944**, *36*, 472–486. [CrossRef]
56. García-Ávila, F.; Ramos-Fernández, L.; Pauta, D.; Quezada, D. Evaluation of water quality and stability in the drinking water distribution network in the Azogues city, Ecuador. *Data Brief* **2018**, *18*, 111–123. [CrossRef]

57. Taghavi, M.; Mohammadi, M.H.; Radfard, M.; Fakhri, Y.; Javane, S. Assessment of scaling and corrosion potential of drinking water resources of Iranshahr. *MethodsX* **2019**, *6*, 278–283. [CrossRef] [PubMed]
58. Shahzad, A.; James, W. Loss in Carrying Capacity of Water Mains due to Encrustation and Biofouling, and Application to Walkerton, Ontario. *J. Water Manag. Model.* **2002**, *volume 10*, 303–324. [CrossRef]
59. Christensen, R.T. *Age Effects on Iron-Based Pipes in Water Distribution Systems. All Graduate Theses and Dissertations (dissertation submitted in partial fulfillment of the requirements for the degree of doctor)*; Utah State University: Logan, UT, USA, 2009; p. 505. Available online: https://digitalcommons.usu.edu/etd/505 (accessed on 11 January 2021).
60. Rollmann, P.; Spindler, K. Explicit representation of the implicit Colebrook-White equation. *Case Stud. Therm. Eng.* **2015**, *5*, 41–47. [CrossRef]
61. Pimenta, B.D.; Robaina, A.D.; Peiter, M.X.; Mezzomo, W.; Kirchner, J.H.; Ben, L.H.B. Performance of explicit approximations of the coefficient of head loss for pressurized conduits. *Revista Brasileira de Engenharia Agrícola e Ambiental* **2018**, *22*, 301–307. [CrossRef]
62. Cengel, Y.A.; Cimbala, J.M. *Fluid Mechanics*, 1st ed.; McGraw-Hill: New York, NY, USA, 2006; pp. 321–398.
63. Shaikh, M.M.; Massan, S.urR.; Wagan, A.I. A new explicit approximation to Colebrook's friction factor in rough pipes under highly turbulent cases. *Int. J. Heat Mass Transf.* **2015**, *88*, 538–543. [CrossRef]
64. Oktaba, W. *Elements of Mathematical Statistics and Experimental Methodology*; PWN: Warszawa, Poland, 1980; p. 310.
65. Barnes, A.A. *Untersuchungen uber die Reibungsziffer Betribsrauher Rohre*; GWF: Essen, Germany, 1959; pp. 289–295.
66. Boxall, J.; Saul, A.; Skipworth, P. Modeling for hydraulic capacity. *J. Am. Water Works Assoc.* **2004**, *96*, 161–169. [CrossRef]
67. Kaur, K.; Annus, I.; Vassiljev, A.; Kändler, N. Determination of Pressure Drop and Flow Velocity in Old Rough Pipes. *Proceedings* **2018**, *2*, 590. [CrossRef]
68. Amouei, A.; Asgharnia, H.; Fallah, H.; Miri, S.; Momeni, H. Evaluating corrosion and scaling potential of drinking water supplies in Juybar, North of Iran. *Iran. J. Health Sci.* **2017**, *5*(2), 11–18. [CrossRef]
69. Shankar, B.S. Determination of Scaling and corrosion tendencies of water through the use of Langelier and Ryznar Scholars Journal of Engineering and Technology (SJET). *Sch. J. Eng. Tech.* **2014**, *2014*, 123–127.
70. Vasconcelos, H.C.; Fernández-Pérez, B.M.; González, S.; Souto, R.M.; Santana, J.J. Characterization of the Corrosive Action of Mineral Waters from Thermal Sources: A Case Study at Azores Archipelago, Portugal. *Water* **2015**, *7*, 3515–3530. [CrossRef]
71. Biglari, H.; Saeidi, M.; Rahdar, S.; Narooie, M.R.; Salimi, A.; Khaksefidi, R.; Baneshi, M.M.; Ahamadabadi, M.; Alipour, V. Evaluation of corrosion and scaling tendency indices in zahedan groundwater resources. *IIOAB J.* **2016**, *7*, 523–528.